Appl. Phys. B 83, 203–211 (2006)
DOI: 10.1007/s00340-006-2148-7

Applied Physics B
Lasers and Optics

K. FURUSAWA[1,✉]
T. OKINO[2]
T. SHIMIZU[1]
H. HASEGAWA[3]
Y. NABEKAWA[1]
K. YAMANOUCHI[2]
K. MIDORIKAWA[1]

Photoelectron spectroscopy of two-photon ionisation of rare-gas atoms by multiple high order harmonics

[1] Laser Technology Laboratory, RIKEN, 2-1, Hirosawa, Wako, Saitama 351-0198, Japan
[2] School of Science, University of Tokyo, Hongo, Bunkyo-ku, Tokyo 113-0033, Japan
[3] Institute for Molecular Science, Myodaiji, Okazaki 444-8585, Japan

Received: 21 December 2005
Published online: 14 March 2006 •

ABSTRACT Two-photon ionisation processes of rare-gas atoms produced by a superposition of multiple high order harmonics are studied by using a photoelectron spectroscopy technique. Second-order nonlinearity is confirmed by comparing the intensity-dependent photoelectron yields between the linear and nonlinear processes, and the cross sections of these processes are estimated. We also demonstrate the autocorrelation measurement of harmonic envelopes as a preliminary step toward characterisation of an attosecond pulse train.

PACS 32.80.Fb; 32.80.Wr; 42.65.-k

1 Introduction

There is a steadily growing interest in nonlinear light–matter interaction studies at EUV/soft X-ray wavelengths. This is owing to the rapid progress in developing novel intense light sources such as X-ray free electron lasers (X-FELs) and laser-based high-order harmonics, the latter of which, in particular, have shown unique potential for probing and steering electrons within an attosecond time scale [1].

Several spectroscopic studies have been reported by using the X-FEL source, where the first experiments on xenon and argon clusters have brought some surprises due to the very efficient energy absorption and ionisation by thermally heated electrons, despite the use of short-wavelength radiation [2]. On the other hand, two-photon double ionisation of helium has been observed by using the intense high order harmonic source at a wavelength of ~ 29.6 nm [3], and which potentially allows us to study the electron-correlation dynamics. For molecules, these ultra-fast short-wavelength sources are expected to enable Coulomb explosion imaging with less distortion than that taken by using near-infrared (NIR) femtosecond lasers owing to the small ponderomotive forces [4].

One of the obvious and interesting opportunities offered by these intense XUV light sources is to observe optical nonlinear effects such as two-photon absorption and four-wave mixing at these wavelengths. Although general considerations on atomic structures suggest that nonlinear cross sections or susceptibilities should be reduced with decreasing wavelengths, nonlinear optical effects are still attractive and useful for developing more sophisticated techniques for studying atomic/molecular dynamics at these wavelengths, as have been harnessed in the visible/near-infrared wavelength range for the past couple of decades. Expecting the rapid progress in developing these intense light sources, some theoretical work has already been conducted [5–7]. This is also important in the context of extending the multiphoton ionisation (MPI) and/or above threshold ionisation (ATI) studies, which have intensively been studied both experimentally and theoretically for the past decade [8], to short-wavelength regimes. Ordinary concepts such as field ionisation become less relevant at these short wavelengths since the ponderomotive energy is extremely small. In addition, the frequency of orbital motions of electrons becomes comparable to or even smaller than the carrier frequency of the pulse, which may lead to significantly different consequences on photoionisation, combined with high intensities. These facts have recently attracted considerable attention as new interests of high- intensity light–matter interaction.

From a practical point of view, optical nonlinearities are useful for autocorrelation measurements of ultra-short optical pulses. Although it has been shown that the cross-correlation measurements between XUV and NIR pulses (via two-colour ATI) are just sufficient for complete characterisation of attosecond XUV pulses [9], it is commonly accepted from the femtosecond metrology that autocorrelation-based techniques generally provide more intuitive understandings for temporal pulse shapes directly from experimental data, since they allow for the shortest temporal sampling in intensity. Characterisation of XUV pulses should become of practical importance when these are to be used for applications. In this regard, it is worth extending the autocorrelation techniques to the XUV regime as not only a counterpart of the cross-correlation-based techniques but also as a means of observing the clear signature of attosecond pulses.

In fact, several groups have reported observation of multiphoton or above-threshold ionisation using high-order harmonics in an XUV/soft X-ray wavelength range [10, 11] and autocorrelation-based pulse characterisation has been performed [12–15]. Some of the authors have performed an autocorrelation measurement at the ever shortest wavelength of 29.6 nm [15] so far. These approaches are primarily categorised into whether ions or electrons are characterised. Whilst they play complementary roles to each other for understanding of the whole process of photoionisation, ion mass

✉ Fax: +81-48-462-4682, E-mail: kf@riken.jp

spectroscopy has more frequently been employed for pulse characterisation [10, 12, 14, 15]. This is partly due to the high collection efficiency readily obtainable from ion mass spectrometers and to the fact that they were mainly intended to characterise a single isolated pulse that possesses a relatively simple spectral structure. However, in our opinion, photoelectron spectroscopy (PES) is a more suitable technique for characterising attosecond pulse trains that result from a superposition of multiple lines of high-order harmonics. Since PES naturally provides spectrally resolved information of the pulse, the contributions from different spectral components (i.e. the individual harmonic orders) can be separately studied to form an attosecond pulse train within the context of Fourier synthesis. Furthermore, by incorporating an interferometer geometry, the resulting delay-dependent photoelectron spectra can be regarded as a spectrogram of the frequency-resolved optical gating (FROG) technique [13], which has widely been used in the femtosecond regime, and can therefore lead to a natural extension to the attosecond regime. However, no detailed characterisation of attosecond pulse trains has so far been reported by using the PES technique.

As a preliminary step toward this goal, we report here the observation of MPI and ATI of rare-gas atoms using multiple lines of intense high-order harmonics (from the 11th to the 15th harmonics of a Ti:sapphire laser) using the PES technique. Using helium and argon as gas samples, their cross sections for the two-photon ionisation processes are estimated by comparing the photoelectron yields between the linear and nonlinear processes. Furthermore, we present an autocorrelation measurement of the pulse envelopes of the harmonics. These data also serve as supplementary information to our recent observation of the attosecond pulse train [16]. In what follows, we first describe our experimental setup in Sect. 2. The single-photon ionisation process of argon is then studied in Sect. 3 in order to determine the spectral distribution of our harmonic source. In Sect. 4, two-photon ionisation processes are studied in terms of spectral profiles and photoelectron yields. We confirm the quadratic intensity dependence of the photoelectron yields and estimate their cross sections. Then, by taking advantage of the two-photon process, a mode-resolved autocorrelation measurement is performed to characterise harmonic pulse envelopes. Finally, conclusions are given in Sect. 5.

2 Experimental setup

In our experiment (see Fig. 1a), we used a Ti:sapphire-based chirped pulse amplification (CPA) system operating at 800 nm, which is capable of producing ~ 40 fs pulses with energies of up to ~ 20 mJ at a repetition rate of 10 Hz. Using this laser as a driver, high-order harmonics were generated by focusing the beam into a static gas cell (10-cm long) filled with xenon (~ 1 Torr) using a lens with a focal length of 5 m. This geometry allows us to obtain harmonics around the 15th order with a total energy of a few microjoules [17]. The intensity of the co-propagating laser beam was reduced by at least three orders of magnitude by using a broadband silicon beam splitter [18] prior to passing through a 4-mm aperture that spatially selects the phase-matched harmonic content [19]. The harmonics around the 13th were then extracted by inserting a tin filter with a thickness of ~ 100 nm (Lebow, 10 lpi mesh). The use of the beam splitter is important for preventing any optical damage to the filter whilst the filter completely eliminates the fundamental laser and low-order harmonic radiation. The harmonic beam was then focused into an interaction region of a magnetic bottle type time of flight (TOF) photoelectron spectrometer [20] by using a silicon carbide mirror with radius of curvature of 100 mm at an incident angle of $\sim 4°$. Theoretically estimated throughputs of these optical components are shown in Fig. 1b. It is expected that the total transmission of the harmonics from the 11th to the 15th (ranging over a bandwidth of ~ 9.3 eV) is more than 5%, and that they compose the major energy content within the interaction volume of the spectrometer. However, we found that the actual transmission coefficients of these components were substantially smaller than the theoretical values as described in Sect. 3.

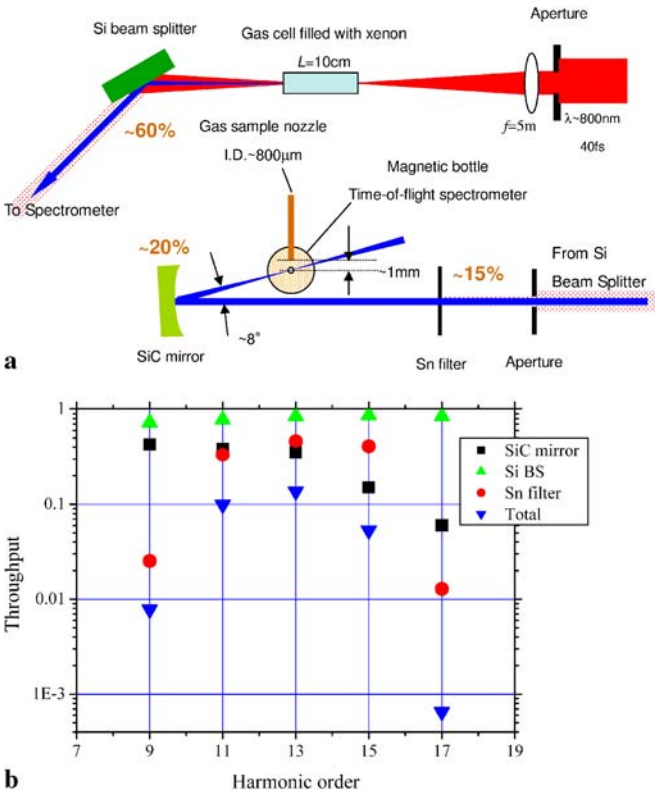

FIGURE 1 (**a**) Experimental setup and (**b**) estimated throughput of the optical components used

A gas sample was supplied to the interaction volume of the spectrometer through a 5-cm-long nozzle ($\sim$ 1-mm I.D.) connected to a pulse valve (General Valve) that was synchronised to the driver laser pulse. The tip of the nozzle was placed just ~ 1 mm above the interaction volume of the spectrometer so as to maximise the gas density when required. A typical background pressure within the interaction chamber was approximately $\sim 10^{-6}$ Torr. This was primarily limited by the xenon gas from the gas cell used for the high order harmonic generation, while the gas leak from the valve itself was negligible as long as moderate back pressures were used (~ 1 atm). The flight tube was isolated from the interaction chamber through a $\sim 700\,\mu$m diameter aperture, from which photoelectrons

enter into the flight tube, and was differentially pumped by a turbo molecular pump (500 l/s). The resultant background pressure within the flight tube was $\sim 10^{-8}$ Torr. The output signal from the spectrometer was monitored by a digital oscilloscope with a bandwidth of 500 MHz at a sampling rate of 5 Gbit/s.

3 Harmonic intensities

We use linear photoelectron spectra of argon in order to quantify the energy content of our harmonic source at the focus. Since an argon atom has its ionisation potential at ~ 15.8 eV, harmonics above the 11th (~ 17.1 eV) can be studied from the photoelectron yields.

The TOF signal $V(t)$ obtained from the spectrometer is approximately related to the harmonic fluence $E(\nu)$ as follows:

$$\int V(t)\mathrm{d}t = eGR\eta\sigma(\nu)N_{\mathrm{atom}}E(\nu)/h\nu, \tag{1}$$

where η is the detection efficiency, $\sigma(\nu)$ is the photoionisation cross section that is a function of the incident photon energy [20], G is the gain of the microchannel plate (MCP), and R is the coupling impedance of the electric signal. N_{atom} is given by $N_{\mathrm{atom}} = PV/kT$, where P, V, k, and T are the pressure, the interaction volume, the Boltzmann constant, and the temperature, respectively. Thus, quantitative measurements can be performed by integrating the TOF signal over an appropriate interval provided that all the parameters are known. Note that we assume here that the bandwidths of the individual harmonics are narrow enough that it is adequate to use a constant cross-section value for a given harmonic and that the TOF spectra are well resolved. η is decomposed into two factors: $\eta = \eta_{\mathrm{geo}}\eta_{\mathrm{MCP}}$. Whilst η_{geo} is ~ 0.5 for our spectrometer [21], η_{MCP} is ~ 0.3 according to the specifications from the manufacturer (Hamamatsu, F1094). The MCP gain is $\sim 10^6$ at 2.0 kV. N_{atom} can be estimated by reading the pressure of an ion gauge within the interaction chamber. The interaction volume is estimated to be 6.1×10^{-8} cm^2 by taking into account the spherical aberrations of the beam. The details are given in Appendix A. Then, the harmonic energies can be deduced from the integrated value of the TOF spectra over an appropriate interval.

Since $E(\nu)$ is proportional to $\int V(t)\mathrm{d}t/\sigma(\nu)$, the relative intensity distribution of the harmonics can be estimated regardless of the measurement conditions. An example is shown in Fig. 2. Although the majority of the energy content concentrates from the 11th to the 15th harmonics, a small amount of energy is still observed above the 17th harmonic. The transmission of the filter was also examined by comparing two photoelectron spectra taken with and without the filter under the same conditions for the sample. The transmission has its maximum at the 15th harmonic and the contrast ratio between the 17th and the 15th harmonics is much smaller than what is expected from Fig. 1b. This indicates that the quality of the filter was degraded possibly due to the surface oxidation induced by the exposure to the atmosphere when it was mounted within our vacuum chamber. We note that the actual transmission coefficients of the optical components used are typically $\sim 50\%$ of the theoretical values, because any small amount of surface contamination leads to significant losses due to the strong absorption at this wavelength range. For this reason, we believe that the photoelectron spectra provide the most reliable information about the energy content of our source within the interaction volume.

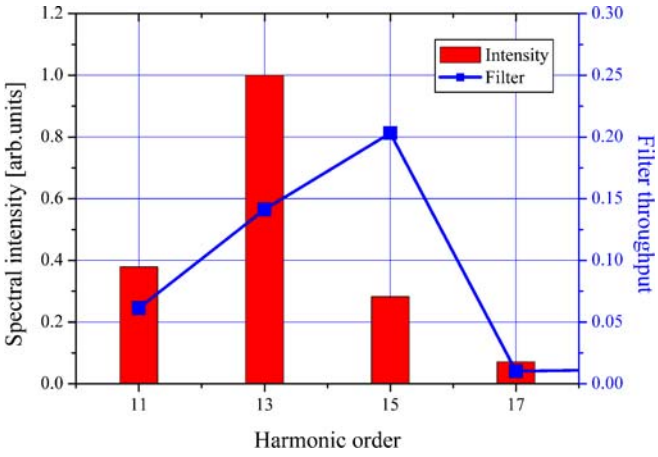

FIGURE 2 Harmonic energy content and filter transmission estimated from the linear photoelectron spectra of argon

For a more quantitative measurement, we take advantage of the gas leaks from the valve. Owing to the strong absorption at these wavelengths and the high sensitivity of our spectrometer, the pressure of the argon gas sample used here was only 4×10^{-6} Torr. The maximum energy of the 13th harmonic at the focus was then estimated to be ~ 45 nJ. Assuming that the total throughput of the optical components used is $\sim 2\%$ including the losses due to the beam splitter ($\sim 60\%$) [18], the filter ($\sim 15\%$), and the mirror ($\sim 20\%$) [23]), the original energy of ~ 2.5 μJ is estimated, in reasonable agreement with the value measured by using an XUV photodiode [17]. Further assuming the pulse duration of 20 fs [16] and the beam radius of about 3 μm at the focus (see Appendix A), the maximum intensity that can be achieved only by the 13th harmonic is then estimated to be 8×10^{12} W/cm^2.

4 Two-photon processes

4.1 *Photoelectron spectra*

The two-photon ionisation processes of helium and argon produced by a superposition of the multiple high order harmonics ranging from the 11th to the 15th are schematically shown in Fig. 3. In both cases, the resulting photoelectrons form multiple peaks in the TOF spectra and their energies can be assigned at even orders (from the 22nd to the 30th) with respect to the fundamental photon energy.

Assuming a coherent superposition of the relevant high-order harmonics and neglecting the wavelength dependence of the photoionisation cross section, the strengths of these photoelectron peaks can be expressed as follows:

$$\begin{aligned} &P_{22} \propto I_{11}^2\,, \\ &P_{24} \propto 4I_{11}I_{13}\,, \\ &P_{26} \propto I_{13}^2 + 4I_{11}I_{15} + 4I_{13}\sqrt{I_{11}I_{15}}\,, \\ &P_{28} \propto 4I_{13}I_{15}\,, \\ &P_{30} \propto I_{15}^2\,. \end{aligned} \tag{2}$$

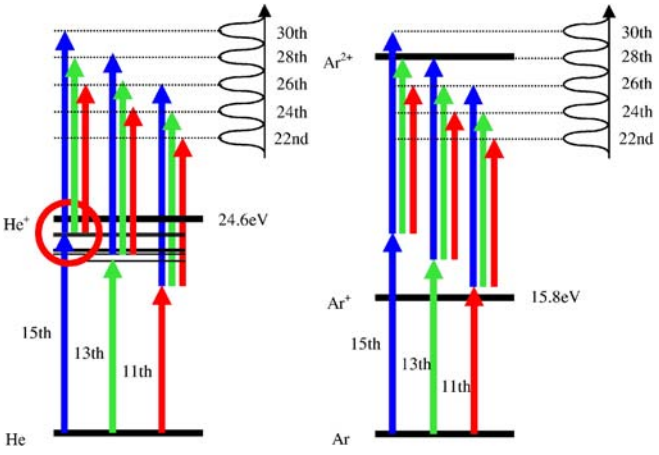

FIGURE 3 Schematic of interactions between the harmonic photons and rare-gas atoms

We omitted the effect of dispersion, since it is expected to be small [16]. P_{26} can be re-written as

$$P_{26} \propto I_{13}^2 \left(1 + 4I_{11}I_{15}/I_{13}^2 + 4\sqrt{I_{11}I_{15}}/I_{13}\right) = I_{13}^2 \left(1 + 4X^2 + 4X\right) . \quad (3)$$

Thus, P_{26}/I_{13}^2 is a quadratic function of a single composite parameter $X = \sqrt{I_{11}I_{15}}/I_{13}$. Thus, it is theoretically possible to quantify the cross sections for each term in (3). However, it turns out that X remain nearly constant over our measurement range as described in Sect. 4.3. Therefore, it is a reasonable approximation to assume that $P_{26} \propto I_{13}^2$ and a single representative cross-section value can then be deduced.

The ionisation potential for helium is 24.6 eV, and thus harmonics above the 17th ($\sim$ 26.4 eV) can directly ionise the neutral helium. Therefore, the interactions between helium atoms and the major energy content of our harmonic source (11th to 15th) can exclusively occur via the two-photon ionisation processes. This is favoured since it makes the interactions less susceptible to the effects of space charges due to the electrons produced via the single-photon ionisation processes. However, the 15th harmonic is likely to overlap with the $1s3p$ states, which can result in some enhancement of photoelectron yields from the 26th to the 30th. Note that this enhancement will degrade the phase sensitivities of these signals when this process is used for autocorrelation measurements.

In contrast, almost all harmonics are subjected to the single-photon ionisation processes for argon since the two-photon processes belong to the ATI processes. In other words, the ATI photoelectrons are necessarily accompanied by an excess amount of photoelectrons generated via the single-photon processes induced by the harmonics from the 11th to the 15th, which may give rise to degradation of resolution in TOF spectra due to the space-charge effects. Thus, by comparing these two atoms, general guidelines for choosing an atomic system suitable for the autocorrelation measurements can be obtained in terms of photon energies of the harmonic source used (i.e. whether they are above or below the ionisation potential of the atoms).

For observing the electrons originated from the two-photon processes, we conducted counting of the signals which exceed a certain threshold voltage within the TOF spectra. By this means, weak signals can be distinguished from background noise by accumulating a large number of data items, which typically amounts to more than 10^4 shots. The retardation voltage of -6 V is applied for argon so as to obtain sufficient energy resolution. On the other hand, we applied an acceleration voltage of 2.8 V for a helium sample so that the difference in potential energy between these two atoms is cancelled out, resulting in similar TOF signals without energy assignment.

The two-photon signals for helium and argon are shown in Fig. 4, where counting was performed over 10^4 shots. A sample gas pressure of 1.4×10^{-3} Torr was used for helium. The 26th signal is the strongest and discrete peaks up to the 30th were observed. The peak corresponding to the 22nd is completely hindered by the presence of one-photon signals at the 21st and 23rd. Note that even the 25th harmonic can be seen since the transmission of the filter at this wavelength is ideally a few percent. However, since the harmonic intensities near the cut-off are extremely sensitive to the driver intensity whilst the harmonics from the 11th to the 15th are not, these higher-order one-photon signals decrease more sharply than the two-photon signals when the driver intensity is slightly reduced. Therefore, these signals can readily be distinguished from the two-photon signals. Note that the one-photon signal can further be suppressed by using a thicker filter, although the achievable intensities by the major harmonic components have to be compromised.

For argon, a gas density of 4×10^{-4} Torr was used. The presence of the one-photon signals near the two-photon signals is less significant compared to that of helium. This is because the photoionisation cross section of argon sharply decreases as the wavelength decreases, and becomes smaller than that of helium for harmonics above the 27th. Combined with the lower gas density used for argon than that for helium, the overlap between the one-photon and two-photon signals is effectively reduced. Nevertheless, we were again unable to observe the peak for the 22nd signal due to the tail of the 21st signal, for which the one-photon ionisation cross section of argon is still four times greater than that of helium.

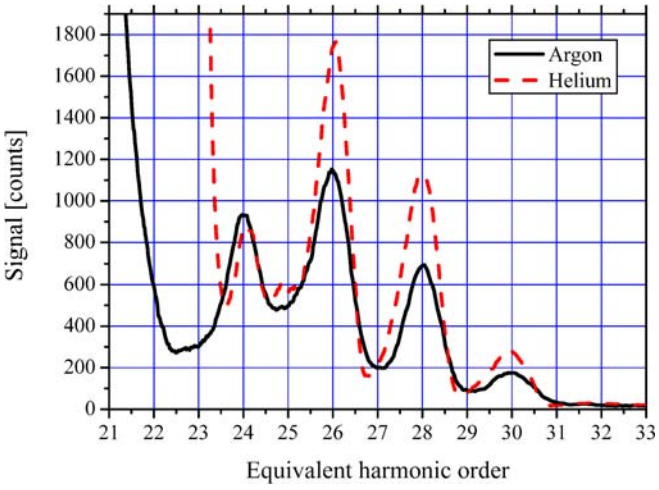

FIGURE 4 Multiphoton signals for helium and argon

When comparing the two-photon signals between these two atoms, the degradation of the resolution in argon is noticeable especially at low equivalent orders. This might be due to the space-charge effect necessarily involved in the ATI processes as described above, but is more likely due to the intrinsic resolution limit set by our spectrometer itself. The intrinsic resolution is primarily determined by the kinetic energies of the resultant photoelectrons, which are greater by ~ 10 eV than those of helium. However, this also seems to mitigate the degree of the space-charge effect, given a much greater number of photoelectrons produced via the single-photon processes in argon.

In terms of distribution of the peaks, the 26th signal is comparable to the 24th signal for argon, qualitatively differing from helium. This implies the presence of the resonant process in helium as described above (see Fig. 3) since the signals above the 26th (26: $15+11$, 28: $15+13$, and 30: $15+15$) may be enhanced relatively to the 24th. Note that a similar process can occur for the 9th harmonic when argon is used as a gas sample. However, since the intensity of the 9th harmonic is well suppressed by the tin filter, as confirmed by the optical spectrometer, this process should be negligible.

4.2 *Intensity dependence*

In order to examine the dependence of the two-photon photoelectron yields on the harmonic intensities, we varied the intensity of the driver laser pulse. This can readily be accomplished by changing the timing of the Q-switched pump laser of the final amplifier within our CPA system. By this means, it is possible to vary the harmonic intensities while changing neither the conditions of the gas cell nor the pulse compressor. Furthermore, the reproducibility of this approach is excellent. Figure 5 shows the delay-dependent harmonic intensities evaluated by using the one-photon signals taken for argon (as described in Sect. 2). The intensities of higher-order harmonics decrease more rapidly with increased Q-switch delay than those of lower orders. This is because the higher-order harmonics are more strongly affected by the intensity of the driver pulses due to the shift of the cut-off energy.

Although it is ideal to monitor both linear and nonlinear processes simultaneously, we found it difficult since the retardation voltage must be applied for argon in order to increase the resolution. This necessarily prevents us from observing the single-photon processes since their kinetic energies are too low. For helium, its ionisation potential is too high to characterise the harmonics 11th and 13th. Thus, other gases that possess smaller ionisation potentials have to be mixed within a gas sample in order to probe these harmonics. However, this complicates the photoelectron spectra and leaves an ambiguity in the sample density.

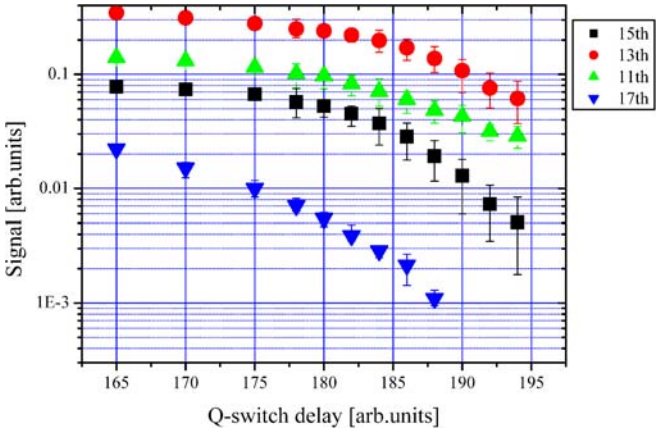

FIGURE 5 Harmonic intensities as a function of Q-switch delay

Therefore, we performed a set of measurements by combining the approaches described in Sects. 3 and 4.1: we first counted the number of photoelectrons from the two-photon processes for various Q-switch delay values, and then subsequently measured the harmonic intensities using the single-photon processes of argon at the same delays. Owing to the excellent reproducibility of the harmonic intensities by the Q-switch delay, combined with the long-term stability of our CPA laser system, we were able to compare the linear and nonlinear processes for given Q-switch delays. We typically accumulated 10^4 shots at each delay to count the two-photon signals and collected the data at ~ 10 different delays. For the one-photon signals, averaged TOF spectra over 10^3 shots are used.

The results are shown in Fig. 6a for helium and Fig. 6b for argon. The gas densities were 4×10^{-4} Torr for helium and 1.5×10^{-4} Torr for argon, respectively. Note that we evaluated the slopes for relevant harmonics according to (2).

In the case of helium, the slope of the 26th harmonic is slightly higher than two. We attribute this to the onset of the one-photon signal at high intensities despite the better resolution intrinsically achievable for helium than for argon. Note that even though all the peaks are resolved, there are finite overlaps between the adjacent peaks, leading to an overestimate of photoelectron counts at high intensities. In contrast, the dependence of both the 28th and the 30th harmonics on the 15th harmonic is slightly less than two, which can be attributed to the following two reasons. Firstly, the reproducibility of the harmonic energies at low driver intensities was not as good as at high intensities, particularly for the 15th harmonic, as observed from the error bars in Fig. 5. Secondly, due to the small number of events (< 100), particularly for the 30th signal, some background contributions within the two-photon signals become non-negligible. Both the 26th and the 28th signals slightly saturate at high intensities. These are primarily attributed to the effects of space charges. Although our spectrometer exhibits particularly good resolution for two-photon signals from helium (9.5–21.9 eV), this also makes the space-charge effects significant.

For argon, all slopes are again nearly two. For the 24th signal, fitting quality is rather poor mainly at low intensities due to the background signals, which are more evident than for helium since the number of photoelectrons generated within the interaction volume is considerably greater than that of helium. At higher intensities, the growth of the 23rd signal is so significant that it contributes to increase the slope of the 24th signal, similarly to the 26th signal of helium. The saturation of the signals is more abrupt than that of helium except for the 30th. However, this is expected because of the strong single-photon ionisation induced by the harmonics from the 11th to the 15th, and which leads

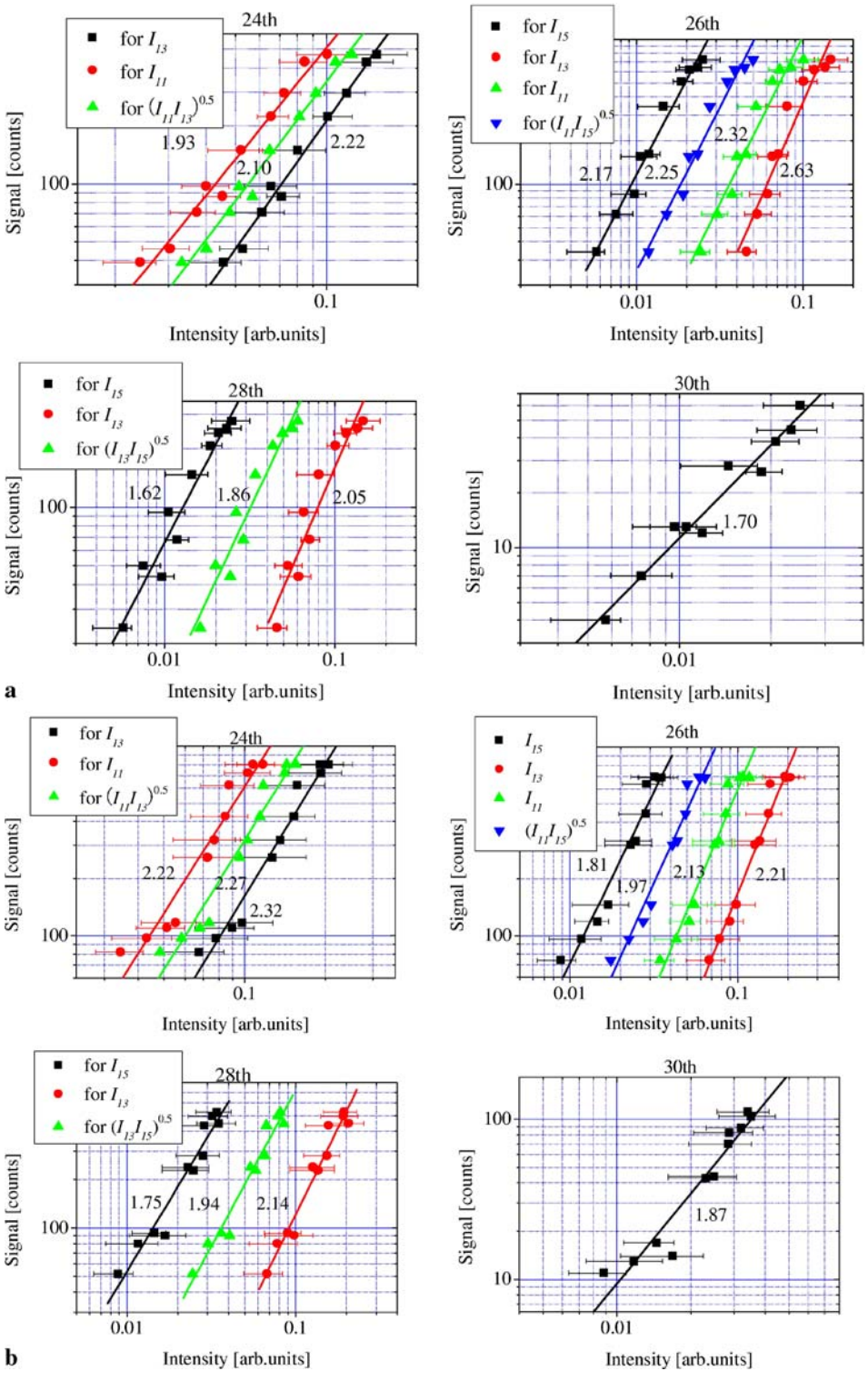

FIGURE 6 Intensity dependences of two-photon signals for helium (**a**) and argon (**b**)

to the depletion of the neutral argon atoms. For instance, the ionisation probability can exceed $\sim 50\%$ for a ~ 45 nJ pulse at the 13th signal if a single 20-fs pulse is assumed. Thus, due to the strong single-photon ionisation processes involved, it is understood that the ultra-short pulse excitation is crucial for observing these two-photon processes for a given pulse intensity. Therefore, this also demonstrates a unique capability of our harmonic source in terms of pulse duration.

4.3 *Cross sections*

In the measurement described above, the number of the counted ATI photoelectrons can be approximated as

$$N_i^{\mathrm{ATI}} = \alpha\eta\sigma_{j,k}^{\mathrm{ATI}} I_j I_k \tau N_{\mathrm{atom}} N_{\mathrm{shots}} / h\nu_j h\nu_k, \tag{4}$$

where $i = j + k$ and $\sigma_{j,k}^{\mathrm{ATI}}$ are the cross sections taking into account the contributions from different harmonic orders. α is a constant that is either unity or four according to (2). Since

	Argon	Helium
$\sigma_{11,13}$	1.6 ± 0.3	0.48 ± 0.08
$\sigma_{13,13}$	3.2 ± 0.8	2.0 ± 0.6
$\sigma_{13,15}$	2.9 ± 0.7	1.0 ± 0.3
$\sigma_{15,15}$	13 ± 2.2	3.7 ± 0.7

TABLE 1 Estimated cross-section values ($\times 10^{-52}$ cm^4 s)

the harmonic intensities I_j and I_k can quantitatively be deduced from the single-photon spectra of argon as described in Sect. 2, the cross-section values for the two-photon processes can also be estimated using the same parameters, except for the interaction volume. Since the nonlinear interactions exclusively occur near the focus, N_{atom} in this case may be expressed as $N_{\text{atom}} = PV_{\text{NL}}/kT = P\pi w_0^2 z_0/kT$, where w_0 and z_0 are the spot size and the Rayleigh length as described in Appendix A. We estimated V_{NL} to be 1.0×10^{-8} cm^3. Using this value, the estimated cross sections for the two-photon processes are summarised in Table 1.

The estimated cross-section values fall within a range between 10^{-53} and 10^{-52} cm^4 s with errors of $\sim 30\%$. In both data sets, the cross-section values tend to be smaller at low equivalent orders such as the 24th and the 26th. We believe that this is reflected by the broadening of the peaks within the TOF spectra especially at low energies due to the space-charge effects, as described above. Note that this directly affects our counting procedure, as we used the peak values of the two-photon signals while neglecting the finite widths of the signals. The X value in (3) takes nearly a constant value of ~ 0.3 at all measurement points, since the sharp variation of I_{15} is compensated for by the slow change of I_{11} while I_{13} exhibits an intermediate character. Consequently, the first two terms in (3) contribute to the 26th signal, resulting in an overestimate for $\sigma_{13,13}$ approximately by a factor of two. Although the values for $\sigma_{15,15}$ are distinctively high, these may represent the most intact values since the signals at the 30th order are the least affected by the effect of space charges. Given these facts, the estimated values are still in reasonable agreement with the theoretical predictions ($\sim 10^{-51}$ cm^4 s) [5].

Compared with argon, $\sigma_{11,13}$ for helium is clearly small. As noticed from the distributions of the two-photon signals in Fig. 4, this suggests that the other values for helium are slightly enhanced due to the $1s3p$ states, although their impacts are not as serious as expected. Note that the theory predicts an order of magnitude enhancement [5] if the wavelength is correctly tuned. Accurate tuning capability of harmonics [24] may allow us to evaluate this effect more accurately, since it strongly depends upon the wavelengths as well as the spectral contents of the harmonics.

4.4 *Autocorrelation measurement*

Relatively large cross sections observed for argon are attractive for autocorrelation measurements and we thus conducted the autocorrelation measurement by using argon. Although the autocorrelation measurement can also be performed using helium, we found some difficulties. Firstly, it was difficult to optimise the two-photon signals while retaining good phase sensitivity with respect to the delay. This implies that the increase of the two-photon signals was accompanied by some blue shifts of the harmonic wavelengths, which reduces the delay sensitivity. Secondly, the two-photon signals from helium are more sensitively affected by the space charges due to the low photoelectron energies involved. To relax this effect, the harmonics above the 17th must be suppressed, whilst maximising the harmonic fluxes below the 15th is crucial for obtaining a sufficient amount of the two-photon signals. Although this also applies to argon, we found that it is possible to obtain more robust and reproducible performance using argon regardless of the spectral distribution of harmonics, compared with helium.

For the autocorrelation measurement geometry, we took advantage of our beam splitter, in order to produce the replica of the pulse [15]. Since the Brewster angle of a Si beam splitter is $\sim 75°$, 1-μm translation amounts to the delay time of ~ 1.7 fs. The delay is scanned every 0.8 μm by accumulating the data over 300 shots at each delay and we repeated this procedure several times. By this means, the long-term stability of

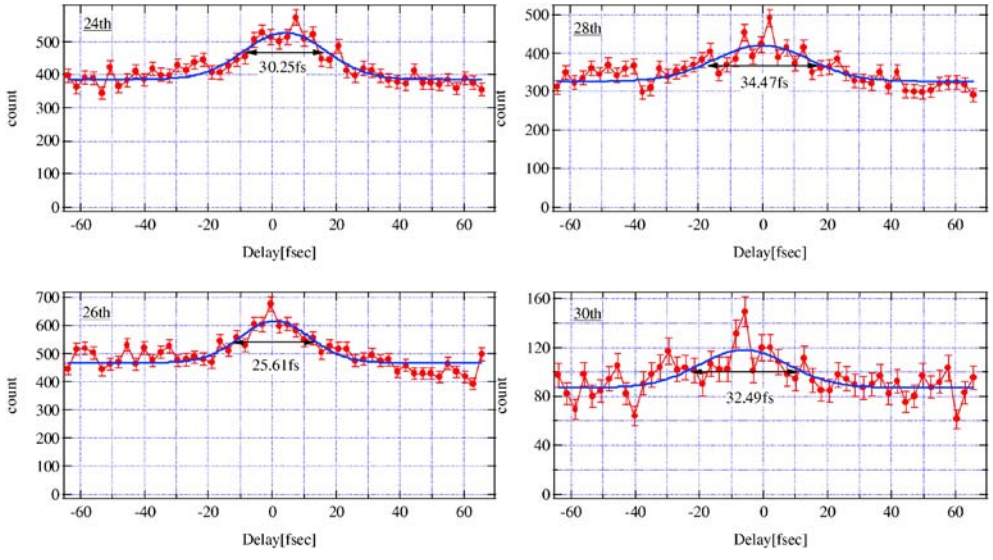

FIGURE 7 Autocorrelation traces of harmonics taken by using argon

the laser intensity can be compensated for. Note that the zero delay was calibrated by taking the autocorrelation of the fundamental prior to this measurement. The result is shown in Fig. 7, where 4000 shots are accumulated at each delay. As we scan the temporal delay, the envelopes of individual peaks are successfully observed. The durations of these envelopes observed vary from 25 fs to 35 fs (FWHM), which is reasonable given the duration of the driver pulse of 40 fs. Although the individual harmonic chirp, which affects the envelope, can in principle be deduced from the shifts of the photoelectron energies at the 24th, 28th, and 30th (for the harmonics from the 11th to the 15th), the resolution was still not good enough. Although this can be overcome by employing a longer flight tube [25], both power and repetition rate scaling of the driver lasers is also essential in order to minimise the degradation of the resolutions. By further decreasing the increment of the temporal delay, the attosecond beating at the 26th harmonic should be resolved, from which the relative phase of individual harmonics can be deduced [16].

5 Conclusions

We have reported the observation of the two-photon ionisation processes produced by the superposition of multiple lines of high-order harmonics via photoelectron spectroscopy. Quadratic intensity dependence of the two-photon signals was confirmed for helium and argon by comparing the one- and two-photon signals despite the space charges and the saturation effects induced by the strong one-photon processes. The cross sections of these two-photon processes have also been estimated. Finally, by taking advantage of this effect, the spectrally resolved autocorrelation measurement is performed to observe the harmonic envelopes. We believe that a clear signature of an attosecond pulse train is obtained by increasing the temporal resolution of our measurement.

Appendix A

In our experiment, the harmonic beam is truncated by an aperture with 4-mm diameter, which determines the initial beam diameter. The beam is then reflected by a spherical mirror with an incident angle of $\theta \sim 4°$. This leads to spherical aberration near the focus as shown in Fig. 8, which can be taken into account by assuming the radii of curvatures as $R\cos\theta$ and $R/\cos\theta$ for orthogonal directions perpendicular to the propagation axis. Furthermore, the M^2 value is known to be ~ 3 [22], which limits the minimum beam diameter. In linear processes, the electrons are produced within the entire volume seen through the 700-μm aperture of the spectrometer. Therefore, the linear interaction volume can be calculated by integrating the effective modal area over this distance, which results in $6.1 \times 10^{-8}\,\mathrm{cm}^3$.

In nonlinear processes, it is adequate to assume that the interactions predominantly occur within the Rayleigh range, which we here define as the distance where the effective modal area becomes twice its minimum value. This distance is estimated to be $\sim 330\,\mu\mathrm{m}$ by taking the spherical aberrations into account, as shown in Fig. 9. Then, by integrating the effective area over this distance, we obtain $1 \times 10^{-8}\,\mathrm{cm}^3$ as a nonlinear interaction volume.

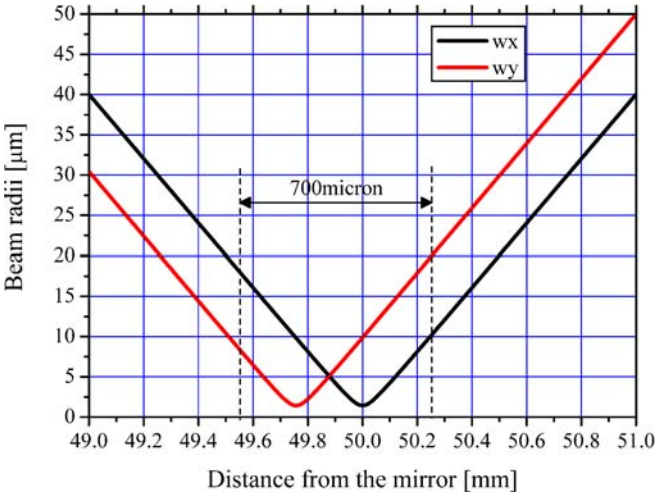

FIGURE 8 The evolution of beam radii along the propagation axis

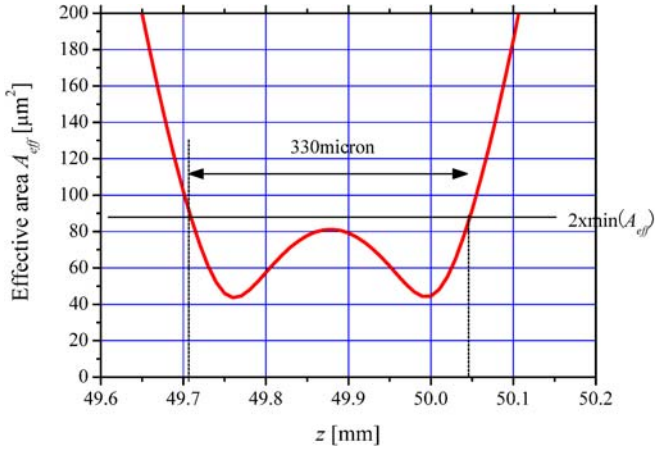

FIGURE 9 The effective mode area near the focus

ACKNOWLEDGEMENTS This research was supported by a Ministry of Education, Culture, Sports, Science, and Technology Grant-in-Aid for Scientific Research on Priority Areas under Grant No. 14077222, a Grant-in-Aid for Young Scientists (A) under Grant No. 16686006, a Grant-in-Aid for Young Scientists (B) under Grant No. 16740237, and by the Special Postdoctoral Researchers Program of the Institute of Physical and Chemical Research (RIKEN).

REFERENCES

1 R. Kienberger, M. Hentschel, M. Uiberacker, C. Spielmann, M. Kitzler, A. Scrinzi, M. Wieland, T. Westerwalbesloh, U. Kleineberg, U. Heinzmann, M. Drescher, F. Krausz, Science **297**, 1144 (2002)
2 H. Wabnitz, L. Bittner, A.R.B. de Castro, R. Dohrmann, P. Gurtler, T. Laarmann, W. Laasch, J. Shulz, A. Swinderski, K. Vonhaeften, T. Moller, B. Faatz, A. Fateev, J. Feldhaus, C. Gerth, U. Hahn, E. Saldin, E. Schneidmiller, K. Sytchev, K. Tiedtke, R. Treusch, M. Yurkov, Nature **420**, 482 (2002)
3 H. Hasegawa, E.J. Takahashi, Y. Nabekawa, K.L. Ishikawa, K. Midorikawa, Phys. Rev. A **71**, 023 407 (2005)
4 A.D. Banderauk, S. Chelkowski, Phys. Rev. Lett. **87**, 273 004 (2001)
5 A. Saenz, P. Lambropoulos, J. Phys. B At. Mol. Opt. **32**, 5629 (1999)
6 T. Nakajima, S. Watanabe, Phys. Rev. A **70**, 043 412 (2004)
7 C. McKenna, H.W. van der Hart, J. Phys. B At. Mol. Opt. **37**, 457 (2004)
8 D. Batani, C.J. Joachiain, S. Martellucci, A.N. Chester (eds.), *Atoms, Solids, and Plasmas in Super-intense Laser Fields* (Kluwer Academic, New York, 2001)

9 F. Quere, Y. Mairesse, J. Itatani, J. Mod. Optic **52**, 339 (2005)
10 N.A. Papadogiannis, L.A.A. Nikolopoulos, D. Charalambidis, G.D. Tsakiris, P. Tzallas, K. Witte, Phys. Rev. Lett. **90**, 133 902 (2003)
11 N. Miyamoto, M. Kamei, D. Yoshitomi, T. Kanai, T. Sekikawa, T. Nakajima, S. Watanabe, Phys. Rev. Lett. **93**, 083 903 (2004)
12 Y. Kobayashi, T. Ohono, T. Sekikawa, Y. Nabekawa, S. Watanabe, Appl. Phys. B **70**, 389 (2000)
13 T. Sekikawa, A. Kosuge, T. Kanai, S. Watanabe, Nature **432**, 605 (2004)
14 P. Tzallas, D. Charalambidis, N.A. Papadogiannis, K. Witte, G.D. Tsakiris, Nature **426**, 267 (2003)
15 Y. Nabekawa, H. Hasegawa, E.J. Takahashi, K. Midorikawa, Phys. Rev. Lett. **94**, 043 001 (2005)
16 Y. Nabekawa, T. Shimizu, T. Okino, H. Hasegawa, K. Furusawa, K. Yamanouchi, K. Midorikawa, submitted to Phys. Rev. Lett.
17 E.J. Takahashi, Y. Nabekawa, K. Midorikawa, Opt. Lett. **27**, 1920 (2002)
18 E.J. Takahashi, H. Hasegawa, Y. Nabekawa, K. Midorikawa, Opt. Lett. **29**, 507 (2004)
19 R. Lopez-Martens, K. Varju, P. Johnsson, J. Mauritsson, Y. Mairesse, P. Salieres, M.B. Gaarde, K.J. Schafer, A. Persson, S. Svanberg, C.G. Wahlstrom, A. L'Huillier, Phys. Rev. Lett. **94**, 033 001 (2005)
20 http://www-cxro.lbl.gov/
21 P. Kruit, F.H. Read, J. Phys. E Sci. Instrum. **16**, 313 (1983)
22 H. Mashiko, A. Suda, K. Midorikawa, Opt. Lett. **29**, 1927 (2004)
23 H. Mashiko, private communication
24 P. Salieres, P. Antoine, A. de Bohan, M. Lewenstein, Phys. Rev. Lett. **81**, 5544 (1998)
25 J.H.D. Eland, O. Vieuxmarie, T. Kinugawa, P. Lablanquie, R.I. Hall, F. Penent, Phys. Rev. Lett. **90**, 053 003 (2003)